Journal of Environmental Chemical Engineering 11 (2023) 110614

Contents lists available at ScienceDirect

Journal of Environmental Chemical Engineering

journal homepage: www.elsevier.com/locate/jece

Superhydrophobic melamine sponges with high performance in oil/organic solvent sorption

Zhihao Dong [a,1], Wenzheng Feng [a,1], Chi Huang [a,1], Hongpeng Lin [a], Chunyan Jia [a,b], Changliang Ren [a,b,*]

[a] Fujian Provincial Key Laboratory of Innovative Drug Target Research and State Key Laboratory of Cellular Stress Biology, School of Pharmaceutical Sciences, Xiamen University, Xiamen, Fujian 361102, China

[b] Shenzhen Research Institute of Xiamen University, Shenzhen, Guangdong 518057, China

ARTICLE INFO

Editor: Pei Xu

Keywords:
Oil spill clean-up
Superhydrophobic materials
Oil/water separation
Melamine sponge

ABSTRACT

The severe adverse impacts of the frequently occurring marine oil spills call for the urgent development of an efficient approach for oil spill restoration. Here, we prepared a superhydrophobic melamine sponge with water contact angle of 151.6° *via* a one-step dip-coating process by simply reacting the melamine sponge with stearic anhydride. The as-prepared sponge, **MS-4**, demonstrates excellent sorption capacities for various organic solvents such as hexane, toluene and chloroform, as well as oils including diesel, mineral oil, and crude oil, with sorption capacities ranging from 78 to 160 times its own mass. Moreover, **MS-4** exhibits good recyclability with retention rate of over 93% even after 50 sorption/squeezing cycles, remarkable stability when exposed to challenging conditions such as strong acidic (pH = 1.0) and alkaline (pH = 13.0) environments, as well as high salinity environments. Additionally, **MS-4** displays superb selectivity, enabling the continuous oil/water separation when assisted by a vacuum pump, achieving a high flux of approximately 10^6 $L \bullet m^{-2} \bullet h^{-1}$, while maintaining a low water content of as minimal as 30 ppm. Notably, through a facile filtration process, **MS-4** achieves an exceptional demulsification efficiency of up to 99.7% for water-in-oil emulsions.

1. Introduction

Frequent occurrence of marine oil spills causes devastating and long-lasting damage to the ocean ecosystem and environment in company with enormous socioeconomic losses [1–3]. The strategies for the treatment of oil spills include booms and skimmers [4], *in situ* burning [5], absorbents [6], dispersant [7], bioremediation [8], solidifiers [9] and phase-selective organogelators [10]. Unfortunately, these strategies suffer from low efficiencies, high costs, complicated oil/water separation steps and introduction of secondary pollution, as well as being time-consuming and difficult in oil reclamation. The serious adverse impacts of oil spills call for the urgent exploration of effective means that allow oil restoration with high performance, low cost, facile operation, oil spill recovery and prevention of secondary contamination. In recent years, porous superhydrophobic materials with outstanding selectivity in oil/water separation, such as carbon nanotube (CNT) sponge [11], porous boron nitride nanosheets [12,13], graphene sponge [14,15], carbon aerogels [16,17] and fibrous membrane [18–20] have received considerable attention. However, their practical application for restoring oily water is mainly hampered by the harsh fabrication conditions, complex multi-step fabrication processes, expensive agents and limited recyclability.

Alternatively, melamine sponge (**MS**) is a low-cost, commercially available material possessing high porosity, low density, high sorption capacity and good elasticity, all of which are desirable features for a high-performance absorbent [21]. Notwithstanding, the pristine **MS** shows an equal sorption preference for oil and water, requiring additional surface modification to achieve desired oil/water separation efficiency. Currently, there are four strategies have been employed for hydrophobic surface modification, including direct carbonization [22], chemical vapor deposition [23], *in situ* chemical reaction [24,25] and dip coating [26–29]. Direct carbonization and chemical vapor deposition strategies typically require high energy consumption, complicated production process and sophisticated equipment, making it impractical

* Corresponding author at: Fujian Provincial Key Laboratory of Innovative Drug Target Research and State Key Laboratory of Cellular Stress Biology, School of Pharmaceutical Sciences, Xiamen University, Xiamen, Fujian 361102, China.
E-mail address: changliang.ren@xmu.edu.cn (C. Ren).

[1] Z. Dong, W. Feng and C. Huang contributed equally to this work

https://doi.org/10.1016/j.jece.2023.110614
Received 6 April 2023; Received in revised form 4 July 2023; Accepted 19 July 2023
Available online 21 July 2023

for large-scale fabrication. The *in situ* chemical reaction strategy typically involves thermal reduction treatment and freeze-dried process, which is also highly costly and requires additional safety investment. Dip coating strategy prepares the hydrophobic **MS** by simply immersing the pristine **MS** several times in the reaction solutions containing modification agents. Compared with the aforementioned three methods, dip coating is more prevailing as it does not need specialized equipment and is easy to operate under mild conditions. However, the existing dip coating strategies for large-scale fabrication are largely restricted by the use of high-cost fluorinated agents, highly active self-polymerizable silanes necessitating fresh preparation, compromised hydrophobicity and/or multi-step coating processes.

In this work, we developed a one-step, economic and scalable approach to fabricate superhydrophobic **MS**s with high performance in oil/water separation under ambient condition. The superhydrophobic **MS**s were synthesized by reacting the secondary amines on the sponge skeletons with acid anhydrides *via* N-acylation reaction under mild condition. The grafted hydrocarbon chains were expected to create a hydrophobic barrier, shielding the **MS** skeletons from the aqueous environment. Meanwhile, they also have the potential to enhance the surface roughness of the **MS**. The successful surface modification was verified by scanning electron microscope/energy dispersive X-ray spectroscopy (SEM/EDS), Fourier transform infrared spectroscopy (FTIR), Raman spectroscopy, X-ray photoelectron spectroscopy (XPS) and thermogravimetric analysis (TGA). The superhydrophobic sponge exhibited excellent sorption capacities up to 160 times its own mass, good recyclability with retention of over 93% after 50 sorption/squeezing cycles, exceptional stability under harsh conditions, superb selectivity enabling continuous oil/water separation and outstanding demulsification ability, which is among the top-notch hydrophobic sponges hitherto reported. The high performance in oil/water separation of this superhydrophobic material in combination with its facile, cost-effective and scalable preparation procedure highlights its great potential in large-scale oil spill remediation.

2. Experimental Section

2.1. Materials

The pristine **MS**s were purchased from the Daiso Industries Co., Ltd., Japan. Acetic anhydride (purity >98%) was purchased from Sinopharm Chemical Reagent Co., Ltd., China. n-Butyric anhydride (purity >98%), n-octanoic anhydride (purity >95%) and diiodomethane (purity >98%) were purchased from Anhui Zesheng Technology Co., Ltd., China. Stearic anhydride (purity >97%) and Span 80 (purity >99%) were purchased from TCI (Shanghai) Development Co., Ltd., China. All organic solvents were purchased from Sinopharm Chemical Reagent Co., Ltd., China. (purity >99.5%) and directly used without further purification.

2.2. Sample preparation

The pristine **MS**s were firstly cut into small cubes ($4 \times 2 \times 1.6\ cm^3$) and soaked in ethanol for 12 h to remove the impurities. After drying in the oven, the pristine **MS**s were immersed in the dichloromethane (DCM) solution containing 10% w/v of different acid anhydrides at 30 ℃ for 24 h. Subsequently, the modified sponges were thoroughly washed with DCM to remove the unreactive acid anhydride residues and dried in oven at 70 ℃ for 12 h. The resultant hydrophobic sponges were denoted as **MS-1, MS-2, MS-3** and **MS-4**, corresponding to the sponges modified with acetic anhydride, n-butyric anhydride, n-octanoic anhydride and stearic anhydride.

2.3. Characterization

Water contact angle (WCA), which is commonly used to assess the surface wettability of materials, was measured using an optical contact angle measuring device (DSA20, KRüSS, Germany). The microstructures of the pristine and modified **MS**s were observed using the field emission scanning electron microscopy (FESEM, Zeiss GeminiSEM 500, Germany). The functional groups in the **MS**s were verified by the Fourier transform infrared spectroscopy (FTIR, Microlet, Japan) and Raman spectroscopy (XploRA, HORIBA, France). The element compositions of the **MS**s were characterized by energy dispersive X-ray spectroscopy (EDS, Ultim Extreme, OXFORD, England) and X-ray photoelectron spectroscopy (XPS) using X-ray spectrometer (ESCALAB Xi+, Thermo Fischer Scientific, USA). The thermal stabilities of the **MS**s were measured by Thermogravimetric Analyzer (Discovery SDT 650, TA Instruments, USA).

2.4. Determination of surface energy

The surface energy of pristine and modified sponges (γ_{MS}) at 20 ℃ was calculated from contact angles ($\cos\theta$) of test liquids by Eqs. (1) and (2):[30].

$$\gamma_l(1+\cos\theta) = 2\sqrt{\gamma_l^p\gamma_{MS}^p} + 2\sqrt{\gamma_l^d\gamma_{MS}^d} \tag{1}$$

$$\gamma_{MS} = \gamma_{MS}^p + \gamma_{MS}^d \tag{2}$$

where γ_l, γ_l^p and γ_l^d are the liquid surface energy, its polar component and dispersive component while γ_{MS}^p and γ_{MS}^d are those of **MS**s, respectively.

Deionized water ($\gamma_l = 72.8\ mN{\bullet}m^{-1}$, $\gamma_l^p = 51.0\ mN{\bullet}m^{-1}$, $\gamma_l^d = 21.8\ mN{\bullet}m^{-1}$) and diiodomethane ($\gamma_l = 50.8\ mN{\bullet}m^{-1}$, $\gamma_l^p = 1.3\ mN{\bullet}m^{-1}$, $\gamma_l^d = 49.3\ mN{\bullet}m^{-1}$) were used as test liquids.

2.5. Sorption, recyclability and flux performance

The sorption capacity, which is defined as the maximum mass of liquid that a given mass of sponge can absorb, was measured *via* the following protocol. Firstly, a piece of modified **MS** ($4 \times 2 \times 1.6\ cm^3$) was immersed in 50 mL of the target oils or organic solvents for 2 min until saturation. Then the saturated **MS** was taken out and quickly weighed. The gravimetric sorption capacity was calculated by Eq. (3):

$$C = \frac{m_{final} - m_{initial}}{m_{initial}} \tag{3}$$

where m_{final} *(g)* is the final mass of **MS**, and $m_{initial}$ *(g)* is the initial mass of **MS**.

The recyclability of modified **MS** was tested by repeated sorption−squeezing processes for 50 cycles and calculated by Eq. (4):

$$R = \frac{D_{50}}{D_1} \times 100\% \tag{4}$$

where D_{50} *(g)* is the saturated sorption capacity after 50 cycles and D_1 *(g)* is the saturated sorption capacity after 1 cycle.

The flux ($L{\bullet}m^{-2}{\bullet}h^{-1}$) of modified **MS** was measured by pouring a variety of oils or organic solvents through a small piece of modified **MS** placed in the funnel. The flux was calculated by Eq. (5):

$$Flux = \frac{V}{A \bullet \Delta t} \tag{5}$$

where V *(L)* is the flow volume, A *(m^2)* is the cross-sectional area at the bottom of the funnel and Δt *(h)* is the time recorded.

2.6. Separation of water-in-oil emulsion

The stable water-in-toluene emulsion was prepared by slowly adding 1.0 mL of water into 100 mL of toluene solution containing 0.1 g of Span 80 under 40 kHz ultrasonic for 5 min, followed by magnetic stirring for

10 h [31]. In the emulsion separation tests, we made a simple filtration device by inserting a modified sponge ($2 \times 2 \times 1.6$ cm^3) into a funnel. The density of **MS-4** was 0.18 ± 0.01 g•cm^{-3}. Then the surfactant-stabilized water-in-toluene emulsion was poured through the compressed **MS-4** and the separation progress was achieved exclusively by gravity. The separation efficiency was calculated by Eq. (6):

$$\eta = \frac{C_{initial} - C_{final}}{C_{initial}} \times 100\% \quad (6)$$

where C_{final} is the final water concentrations in emulsion, and $C_{initial}$ is the initial water concentrations in emulsion. The emulsion droplets distribution before and after filtration were measured *via* dynamic light scattering (DLS, Zetasizer Nano-ZS 90, Malvern, UK). The moisture contents before and after separation were determined using an automatic micro-moisture tester (ST-1513A, Beijing Xuxi, China).

3. Results and discussion

3.1. Wettability of modified sponges

The commercially available pristine **MS** is a three-dimensional (3D) porous structure composed of cross-linked formaldehyde-melamine-sodium bisulfite. The secondary amines in the skeletons would account for its hydrophilicity and in the meanwhile open up the possibility for surface modification. We proposed that reacting the secondary amines of pristine **MS** with acid anhydrides *via* N-acylation reaction would result in two significant effects. On the one hand, it leads to a reduction in the N-H•••O hydrogen bonding interactions between the **MS** skeletons and water, resulting in a decrease in surface energy. This reduction facilitates the creation of a hydrophobic barrier that effectively shields the **MS** skeletons from the surrounding aqueous environment. On the other hand, this reaction has the potential to enhance the surface roughness of the **MS**. As surface chemistry and surface topography are the two critical factors that govern the wettability of the surface, this strategy would effectively transform the initially hydrophilic surface into a more hydrophobic one, as illustrated in Fig. 1 [32]. To test our hypothesis, we initially dipped the pristine **MS** in a dichloromethane solution containing 10% w/v of acetic anhydrides at 30 ℃ for 24 h. The modified sponge was thoroughly washed with dichloromethane and dried in oven at 70 ℃ for 12 h. To our delight, this simple approach worked as expected. Fig. 2a showed the behavior of water droplets on the surface of the pristine **MS** and **MS-1**. When diesel (dyed with Sudan III) and water (dyed with methylene blue) were dropped on the surface of the pristine **MS**, both liquids were absorbed immediately. However, when water was dropped on the surface of **MS-1**, it could stay on the surface of the sponge and reserve a relatively intact spherical shape. On the contrary, the diesel droplet was instantly absorbed. The wettability, which is an essential standard for accessing the hydrophobicity of the N-acetylated **MS** (**MS-1**), was measured by the water contact angle (WCA). As shown in Table 1, **MS-1** exhibited good hydrophobicity with WCA measured to be $138.5 \pm 2.5°$. The surface energy of **MS-1** was determined to be 8.6 mN•m^{-1}, exhibiting a substantial reduction compared to the pristine **MS** with a surface energy of 93.2 mN•m^{-1}. This result undoubtedly substantiated our initial proposal that N-acylation of secondary amines could be a promising strategy to reduce the surface energy of **MS**. Encouraged by this exciting result, we further expanded our study by reacting **MS** with n-butyric anhydride, n-octanoic anhydride or stearic anhydride to explore the impact of hydrocarbon chain length on the hydrophobicity of melamine sponges. As shown in Fig. 2b and summarized in Table 1, extending the length of the grafted hydrocarbon chains tended to decrease the surface energy of the as-prepared sponges as a general trend. Most importantly, **MS-4**, which was fabricated by reacting pristine **MS** with stearic anhydride, demonstrated impressive superhydrophobicity with a WCA of $151.6 \pm 2.4°$. The superior water repellency of **MS-4** was further demonstrated by the floating experiments. When the pristine **MS** was placed onto the surface of water, it could quickly absorb water and sink to the bottom (Fig. 2c). In sharp contrast, **MS-4** could stay afloat above the water (Fig. 2d). When external force was applied to immerse **MS-4** in the water, we observed mirror-like interfaces formed by entrapped air at the interface of **MS-4** and the surrounding aqueous environment as a result of the Cassie-Baxter non-wetting behavior (Fig. 2e) [33]. Once the external force was released, **MS-4** immediately refloated to the surface of water in an anhydrous manner.

3.2. Characterization

3.2.1. SEM and EDS analysis

The morphologies of the pristine **MS** and **MS-4** were visualized by SEM. As illustrated in Fig. 3a, the pristine **MS** was made up of melamine cross-linking networks with a 3D porous structure and smooth skeletons. The pore size ranged from 150 to 200 μm and the skeletons showed an average diameter of ~ 6 μm. After modification with stearic anhydride, **MS-4** retained the similar porous structure, skeleton dimensions, confirming that the mild reaction condition did not alter the intrinsic morphology of sponges (Fig. 3c). However, in contrast to the pristine **MS**, which demonstrated a smooth surface on its skeleton, **MS-4** exhibited a substantial presence of nano-sized extrusions (ranging from 60 to 140 nm) coated on the skeleton surface, clearly indicating a notable enhancement in surface roughness for the modified sponge. In comparison to a smooth surface, water droplets deposited on the surface of enhanced roughness exhibit a propensity to reflect the Cassie-Baxter model in the open air regime, which gives rise to multiple metastable equilibrium positions for the water droplets, enabling their facile transfer between these positions. Additionally, it is also possible for water droplets to exhibit characteristics in accordance with the Wenzel model, where the droplets conform and spread into the micro-scale asperities of the rough surface, leading to an increased contact area between the droplets and the surface [34]. Consequently, both of these phenomena would contribute to the development of the

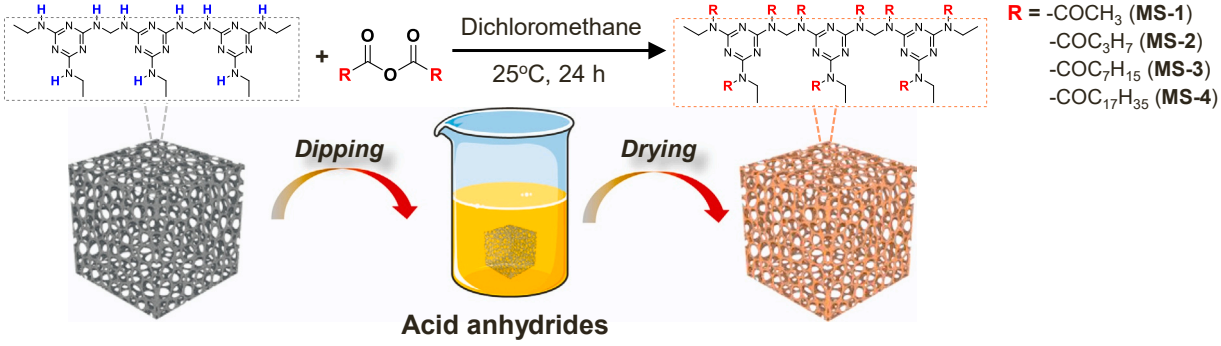

Fig. 1. Schematic illustration of the N-acylation of a pristine melamine sponge.

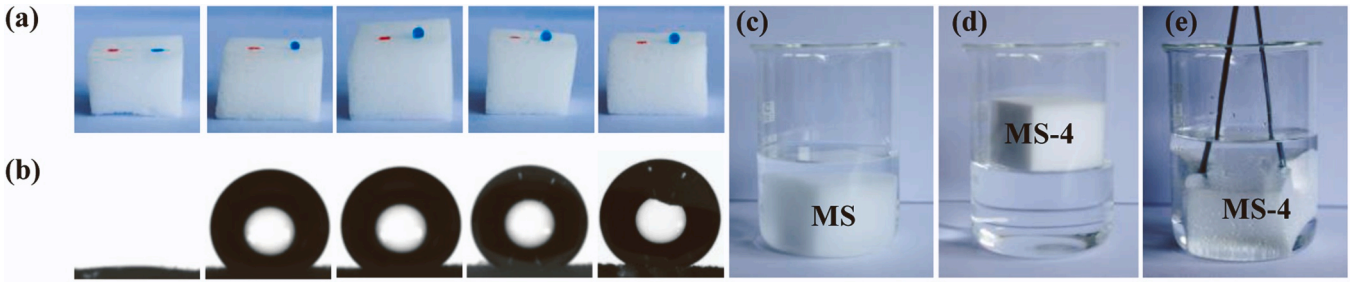

Fig. 2. Photographs of (a) diesel (dyed with Sudan III) and water (dyed with methylene blue) droplets on the surface of the pristine **MS**, **MS-1**, **MS-2**, **MS-3** and **MS-4** (from left to right); (b) the water contact angles of the pristine **MS**, **MS-1**, **MS-2**, **MS-3** and **MS-4** (from left to right); (c, d) the pristine **MS** and **MS-4** being placed on the surface of water and (e) **MS-4** was forced into water to present mirror-like interfaces.

Table 1
Contact angle (°) and the surface energy (mN•m^{-1}) of the pristine and modified **MS**s (20 ℃).

Samples	Contact angle (°)		Surface energy (mN•m^{-1})
	Water	Diiodomethane	
MS	0	108.8 ± 3.0	93.2
MS-1	138.5 ± 2.5	103.4 ± 3.8	8.6
MS-2	142.3 ± 1.6	109.5 ± 3.5	6.6
MS-3	142.4 ± 1.2	111.5 ± 1.4	5.9
MS-4	151.6 ± 2.4	125.8 ± 0.6	2.6

superhydrophobic property of **MS-4**. Additionally, EDS analysis was performed using the point scan model in images obtained by SEM. According to the data presented in Fig. 3b, the weight percentages of C, N and O which were the main elements in **MS** were determined to be 48.8%, 46.5% and 3.9%, respectively. After modification, it was observed that the weight percentages of C and O in **MS-4** were dramatically enhanced to 62.3% and 8.2%, respectively (Fig. 3d), indicating high possibility of the successful attachment of the stearoyl chains onto the melamine skeletons.

3.2.2. XPS analysis

X-ray photoelectron spectroscopy (XPS) was applied to further analyze the chemical composition and bond formation in both pristine **MS** and **MS-4**. As illustrated in Fig. 4a, the main peaks detected at 285.98, 398.96 and 532.22 eV corresponded to the binding energies of C1s, N1s and O1s, respectively. The acylation reaction with stearic anhydride resulted in a substantial rise in the relative height of C1s. The area ratio of the C1s/N1s peak increased from 1.41 to 6.55 and the ratio of C1s/O1s peak increased from 1.85 to 2.74, revealing that the stearoyl group, which contained one oxygen atom and eighteen carbon atoms but no nitrogen atom, was unambiguously introduced to the sponge. Details of the deconvoluted peaks of C1s, N1s and O1s showed that surface modification gave rise to a significant enhancement to the relative intensities of the C−C bond at 284.8 eV, the N − C bond at 399.3 eV and the carbonyl group at 531.5 eV (Fig. 4b to g), providing additional evidence for the presence of the C−C bond-rich stearoyl groups and formation of amide bonds.

3.2.3. FTIR and Raman analysis

Moreover, FTIR and Raman spectroscopies were performed to examine the successful covalent modification on the **MS** skeleton surface. As shown in Fig. 5a, the FTIR spectra of pristine **MS** displayed prominent bands at 809, 1142, 1545 and 3381 cm^{-1}, attributed to the bending vibration of triazine ring and stretching vibrations of C−O, C═N and secondary amine N − H, respectively [35]. The bands at 1326 and 1458 cm^{-1} corresponded to the bending vibrations of C−H in the -CH_2- groups, whereas the band at 2924 cm^{-1} was ascribed to the C−H stretching vibration. In comparison, the spectra of **MS-4** exhibited

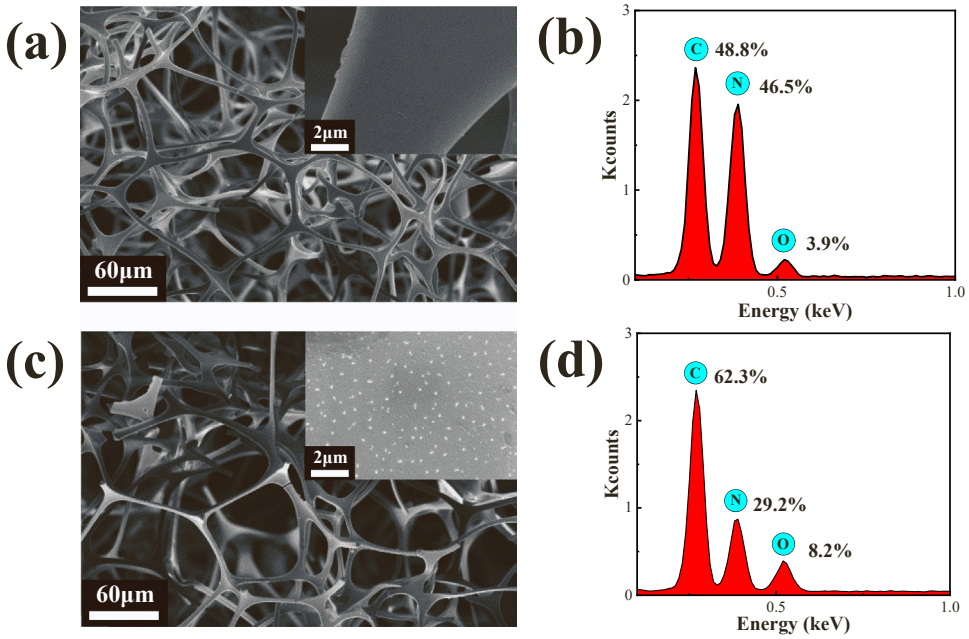

Fig. 3. SEM images of the pristine **MS** (a) and **MS-4** (c); EDS diagrams of the pristine **MS** (b) and **MS-4** (d).

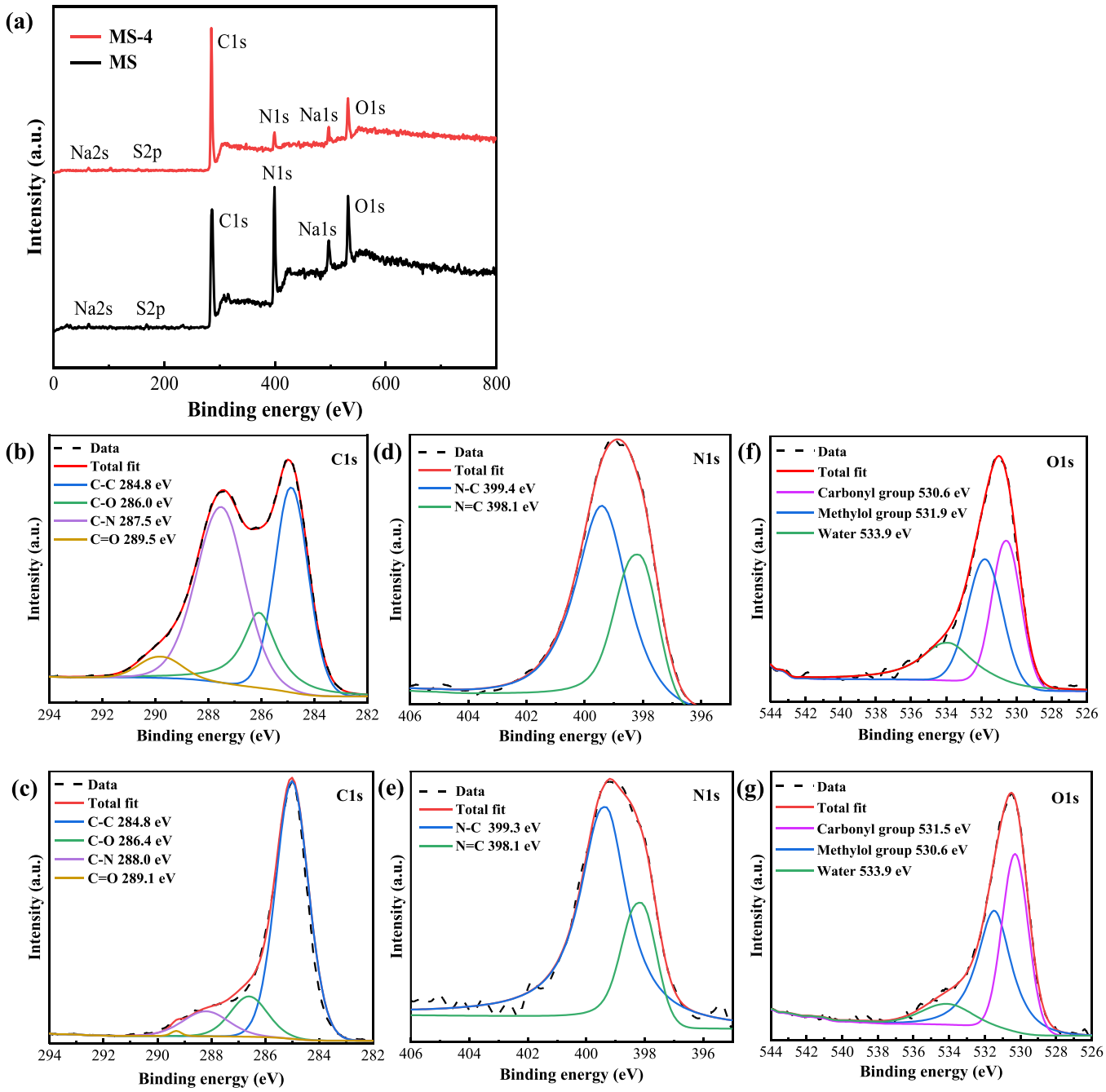

Fig. 4. (a) Full XPS spectra of the pristine **MS** and **MS-4** and fitting of the XPS C1s, N1s and O1s peak of (b, d, f) the pristine **MS** and (c, e, g) **MS-4**.

additional C═O stretching band obviously appeared at 1698 cm^{-1} with decreased intensity of the N−H stretching bands, indicative of the successful formation of amide bonds. Meanwhile, significant enhancement of the intensity of C−H stretching bands at 2916 and 2849 cm^{-1} further verified the successful grafting of long alkyl chains on the sponge surface.

Fig. 5b illustrated the Raman spectra of the pristine **MS**, revealing the presence of N−H, C−H and triazine rings at 3425, 2970 and 973 cm^{-1}, respectively, as well as C−H and C−N bending vibrations at 1438 cm^{-1} and 743 cm^{-1}, respectively [36]. The modification process resulted in the disappearance of the N−H stretching band, the appearance of the C═O stretching band at 1797 cm^{-1} and the increase of the C−H stretching band, which additionally confirmed the formation of amide bonds. Furthermore, three new bands observed at 1293 cm^{-1}, 1126 cm^{-1} and 1067 cm^{-1} were assigned to the in-phase CH_2 twist, C−C−C symmetric and asymmetric stretching bands, respectively [37]. These results, in combination with the FTIR analysis, provided collective evidence of the successful covalent modification of long alkyl chains onto the **MS** skeletons through amide bond formation.

3.2.4. *Degradation behavior analysis*

The degradation behavior of pristine **MS** and **MS-4** were analyzed by thermogravimetric analysis (TGA) under N_2 atmosphere (Fig. 6). The mass loss curve of **MS-4** could be assigned into three temperature ranges. The first mass loss of ~ 6% at the temperature below 100 ℃ was attributed to the evaporation of absorbed water in the sponges. The second mass loss of ~ 27% within the temperature range of 360–410 ℃ was attributed to the thermal degradation of methylene bridges. The third mass of ~ 38% loss at the temperature over 410 ℃ was attributed to the thermal degradation of triazine rings. When compared to the

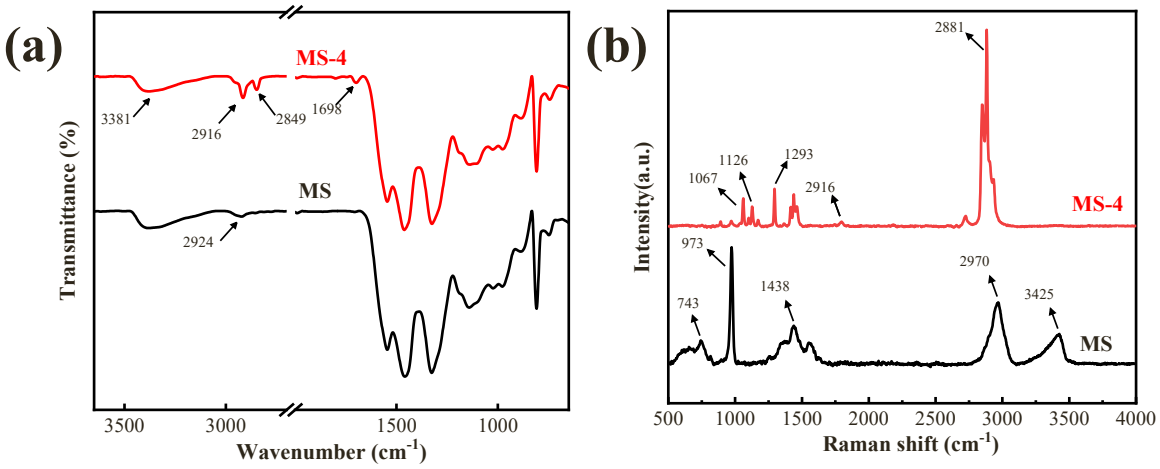

Fig. 5. FTIR (a) and Raman (b) spectra of the pristine **MS** and **MS-4**.

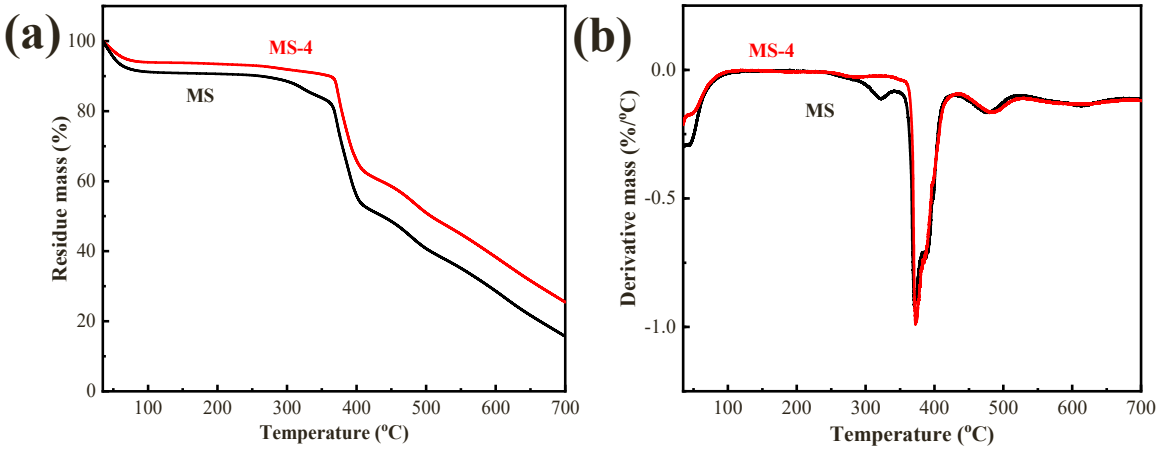

Fig. 6. TG (a) and DTG (b) curves of the pristine **MS** and **MS-4**.

degradation behavior of the pristine **MS**, **MS-4** demonstrated a smaller mass loss of ~ 3% in the first mass loss range, suggesting a lower sorption of water due to the improved hydrophobicity.

3.3. Mechanical and chemical stability

In addition to thermal stability, the practical application of **MS-4** also depends on its mechanical and chemical stability. To access the mechanical stability, a universal testing machine (microtester 5948, Instron ITW, England) was employed to conduct repeated tests at a compression rate of 10 mm/min. The results depicted in Fig. 7a revealed that **MS-4** could recover its original shape even after being subjected to 80% strain. Meanwhile, **MS-4** exhibited a plastic deformation of only 7.5% after undergoing 100 cycles of 60% strain (Fig. 7b), implying its exceptional flexibility and mechanical stability. The SEM images shown in Fig. S2 depict the increasing degree of fracture in the sponge skeleton structure as the compression cycles are increased. The observed changes in the mechanical properties may be attributed to this progressive fracturing of the sponge skeleton structure. Also, we tested the WCAs of **MS-4** after undergoing 50 cycles of sorption/squeezing processes for a variety of oils or organic solvents. The results showed that the WCAs of **MS-4** maintained 145.8–151.6° despite experiencing repeated sorption/squeezing processes (Fig. S2). The chemical stability was further evaluated by measuring the WCAs after soaking **MS-4** in aqueous solutions at varying pH (1, 4, 7, 10 and 13). As depicted in Fig. 7c, acidic and alkaline solutions exhibited minimum influence on the WCAs of **MS-4**, implying the excellent resistance of **MS-4** towards acidic and alkaline environments. Moreover, **MS-4** also remained excellent hydrophobicity with WCA of 149.3°, even upon the exposure to a 40% sodium chloride solution (Fig. 7d). The impressive mechanical and chemical stability highlighted the potential applications of **MS-4** under harsh conditions.

3.4. Sorption capacity, recyclability and flux performance

The exceptional porosity and superhydrophobicity of **MS-4** prompted us to conduct a comprehensive assessment of its sorption capacities and recyclability for oils/organic solvents, which were the two key criteria for a desirable oil spill remediation material. The sorption capacities of **MS-4** for 5 oils and 6 organic solvents with different densities and viscosities in the absence of water were summarized in Table 2. As can be seen, **MS-4** exhibited exceptional sorption capacities, achieving as high as 78–160 times its own mass depending on the densities of tested liquids. The sorption performance of **MS-4** was superior to those of wool [38], nanowire membrane [39] and conventional polymer absorbents [40], and was clearly among the best performing superhydrophobic sorbent materials hitherto reported [41,42] (Table 3).

Furthermore, we performed intermittent sorption experiments to determine the sorption kinetics for oils/organic solvents. The sorption capacity curves for crude oil, mineral oil and peanut oil with viscosity > 20 mPa•s are depicted in Fig. S4. The experimental results revealed that the sorption of **MS-4** towards crude oil, mineral oil and peanut oil reached saturation within 15, 25 and 35 s, respectively. For the other 8

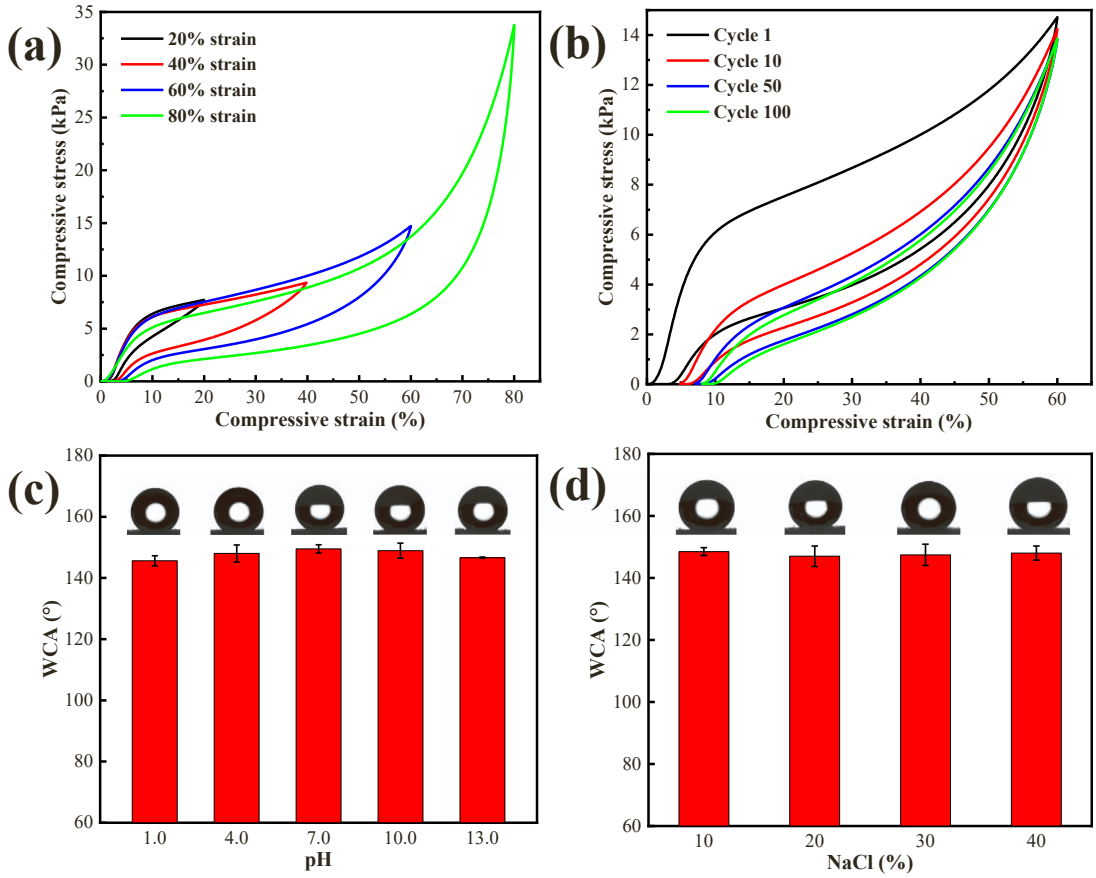

Fig. 7. (a) Compressive stress-strain curves of **MS-4** at different strains (20%, 40%, 60% and 80%); (b) Cyclical stress-strain curves of **MS-4** at 60% strain for 100 cycles; water contact angles of **MS-4** after soaking in solutions with different pH values (c) and concentrations of sodium chloride (d) for 24 h.

Table 2
Sorption capacity, recyclability after 50 cycles of sorption−squeezing process and flux of **MS-4** for various organic solvents or oils.

	Density (g/cm^3)	Sorption capacity (g/g)	Sorption capacity in oil-water mixture (g/g)	Sorption capacity retention after 50 cycles (%)	Flux ($L{\cdot}m^{-2}{\cdot}h^{-1}$)
Hexane	0.67	78.1	77.6	97.4%	7.2×10^5
Toluene	0.87	92.4	90.9	99.5%	5.8×10^5
THF	0.89	105.5	-[a]	93.2%	7.3×10^5
Ethyl acetate	0.90	107.0	103.5	96.1%	7.4×10^5
DCM	1.33	135.0	136.9	99.1%	8.9×10^5
Chloroform	1.48	159.5	158.7	96.7%	8.0×10^5
Gasoline	0.74	87.2	86.0	97.2%	6.4×10^5
Diesel	0.82	86.5	83.8	98.3%	5.9×10^4
Mineral oil	0.84	84.7	87.1	95.5%	3.2×10^3
Crude oil	0.90	107.8	115.8	95.6%	1.2×10^2
Peanut oil	0.91	89.7	91.8	96.1%	2.5×10^3

[a] miscible with water

oils/organic solvents with viscosity < 6 mPa•s, the sorption of **MS-4** reached saturation within 5 s. It is interesting to note that the sorption rate is inversely proportional to the viscosity of the respective oils/organic solvents. This may be attributed to the unique 3D interconnected network structure of **MS-4**. Owing to this structure, oils/organic solvents with lower viscosity are able to readily penetrate and spread throughout the entire sponge *via* the porous framework. In contrast, oils with higher viscosity encounter greater resistance in permeating the sponge structure, resulting in a slower sorption. The viscosities of the studied oils/organic solvents are summarized in Table S1.

An additional noteworthy advantage of our preparation protocol is the capacity of the reaction reagents that can be repeatedly utilized over 10 times without compromising the hydrophobicity of the as-prepared sponges (Fig. S3). This merit facilitates the large-scale manufacturing of the superhydrophobic melamine sponge at considerably reduced costs, thereby allowing for the cost-effective treatment of 1 liter of spilled oil at approximately $1 (for a detailed calculation of the preparation cost of **MS-4**, please refer to Note 1 in the supplementary information). Moreover, **MS-4** also demonstrated notable recyclability by retaining more than 93% of its original sorption capacities for all the tested liquids after 50 cycles of sorption/squeezing processes. The slight decrease in sorption capacities might result from the existence of residue solvents inside the sponge which were not be fully eliminated by manual squeezing. The flux performance of **MS-4** towards various oils or organic solvents was also evaluated in this study. As summarized in Table 2, **MS-4** demonstrated good flux performance for a wide range of oils or organic solvents, with values ranging from 5.9×10^4 to 8.9×10^5 $L{\bullet}m^2{\bullet}h^{-1}$. For oils with increased densities, such as mineral oil, crude oil and peanut oil, the flux was observed to decrease, with values ranging from 1.2×10^2 to 3.2×10^3 $L{\bullet}m^2{\bullet}h^{-1}$.

3.5. Selective sorption performance

Apart from sorption capacity and recyclability, the selectivity of oil sorption also plays a pivotal role in practical oil/water separation. To explore the efficiency, we introduced diesel (dyed with Sudan III) into the seawater to simulate oil spill and placed **MS-4** to the oil/water mixture. As soon as **MS-4** contacted the mixture, it rapidly absorbed

Table 3
Modification strategies for hydrophobic melamine sponges.

Type of melamine sponge	Modification strategy	Sorption capacity (g/g)	WCA (°)	Ref.
m-CNT/PPy modified MS	In situ chemical reaction	32–97	158	[43]
PDA/SC modified MS	In situ chemical reaction	82.9–173.8	165.9	[44]
Urushiol modified MS	In situ chemical reaction	88.3–181.7	131	[45]
ZIF-8 modified MS	In situ chemical reaction	10–38	140	[46]
USTC-6 @GO modified MS	In situ chemical reaction	12–43	132	[47]
PDA/DDT modified MS	In situ chemical reaction	45.2–98.6	158	[48]
PDA/1 H,1 H,2 H,2 H-perfluorodecanethiol modified MS	In situ chemical reaction	79–195	163.4	[49]
PDA/Fe_3O_4/Ag/ODA modified MS	In situ chemical reaction	55.9–99.6	156.3	[50]
Lignin modified MS	Carbonization	98–217	142.5	[51]
Carbonized resol modified MS	Carbonization	88–204	146	[52]
Carbonized asphalt modified MS	Carbonization	73–140	134.5	[53]
Melamine-derived carbon sponge	Carbonization	90–200	140	[54]
PPy−PTES modified MS	Chemical vapor deposition	21.8–31	153.7	[55]
MF/PPy/Ag/F modified MS	Chemical vapor deposition	37–97	156.1	[56]
PCL/PDLLA modified MS	Dip coating	3.3–8.8	162	[28]
CB[6] modified MS	Dip coating	53–112	112.7	[27]
PDVB-PDMS modified MS	Dip coating	16.45	153	[57]
Graphdiyne modified MS	Dip coating	75–160	130	[58]
WPAC modified MS	Dip coating	78–172	153.5	[41]
MS-Eucalyptol:Menthol (1:5) modified MS	Dip coating	96.1–132.2	152	[59]
Silanized modified MS	Dip coating	82–163	151	[35]
PDMS modified MS	Dip coating	45–75	> 150	[60]
PODS modified MS	Dip coating	42–68	153	[61]
MoS_2@RTV modified MS	Dip coating	56–104	152	[62]
Few layer graphene modified MS	Dip coating	57–153	143.5	[63]
MWCNTs-PDMS modified MS	Dip coating	38–127	159.8	[64]
Furfuryl alcohol modified MS	Dip coating	75–160	145	[65]
Poly(phenol-amine) modified MS	Dip coating	71–147	> 150	[66]
MS-4	Dip coating	78–160	151.6	This work

diesel within a few seconds and floated on the surface of seawater, leaving a clear aqueous layer unaffected. This result demonstrated the excellent selectivity of **MS-4** for oil sorption (Fig. 8a). Subsequently, the absorbed oil could be easily reclaimed by squeezing process. Similarly, we investigated the selective sorption performance of **MS-4** towards chloroform with density greater than water, for the purpose of evaluating its water immersion resistance and underwater sorption performance. Fig. 8b demonstrated the outstanding water immersion resistance of **MS-4**, coupled with its impressive capacity to efficiently absorb chloroform even when fully immersed in water. Following this positive result, we further examined the selective sorption capability of **MS-4** towards a wider range of biphasic mixtures. Encouragingly, **MS-4** still retained over 95% of its original sorption capacities for all of the tested oils or organic solvents (Table 2), highlighting its promising application to efficiently remove various oils or organic solvents in the presence of water.

We expected that an automatic device equipped with the superhydrophobic **MS-4** as oil filter enabling continuous oil/water separation should be more intelligent for large-scale oil spill clean-up and recovery. Therefore, a device was assembled by connecting **MS-4** to a collection flask *via* a rubber tube. When external vacuum was applied (vacuum pump, GM-0.5B, Jinteng Instrument Co. Ltd., China, pressure: −0.095 MPa), 200 mL of diesel could be fully recovered within 40 s whist the total volume of water remained unchanged even when the sponge was immersed in the water (Fig. 8c). The flux of diesel in continuous oil/water separation experiments were calculated to be 1.2×10^6 $L•m^{-2}•h^{-1}$. The water content of diesel after separation was determined to be 24.6 ± 0.2 ppm using an automatic micro-moisture tester. Despite the oil/water mixture was vigorously stirred to generate a more turbulent environment, the high performance of the device for oil/water separation was seldom compromised (Fig. 8d). The flux of oil in continuous oil/water separation experiments under vigorous stirring were calculated to be 9.7×10^5 $L•m^{-2}•h^{-1}$. The water content of diesel after separation was determined to be 30.2 ± 1.1 ppm. These results indicated the feasibility to use **MS-4** to achieve a labor-free *in situ* oil/water separation even in rough water.

3.6. Demulsification of water-in-oil emulsion

Separation of emulsion is a more challenging task as compared to that of immiscible oil/water mixtures [67]. Interestingly, the efficient separation of water-in-oil emulsion using **MS-4** could be achieved through a simple filtration process which involved the use of a filter funnel fitted with **MS-4** (Fig. 9). When the water-in-toluene emulsion was poured through the funnel, transparent toluene could be obtained with a flux of 7.1×10^2 $L•m^{-2}•h^{-1}$. The image of demulsified emulsion recorded by optical microscope displayed a high clarity, which was notably distinct from the image of the water-in-toluene emulsion, where a plethora of emulsified droplets were observed. Using dynamic light scattering (DLS), the average droplet size was measured to be 790 nm. However, after separation, the droplet size became too small to be detected by DLS, further highlighting the high separation efficiency of **MS-4**. The demulsification process is facilitated by the superhydrophobic and superoleophilic characteristics of the surface and the capillary forces within the sponge's pores. Consequently, the peripheral oil surrounding the emulsion droplets is drawn into the sponge due to capillary action, while the water encapsulated within the droplets is repelled [68,69]. Finally, we calculated the separation efficiency using an automatic micro-moisture tester which showed that over 99.7% of the water could be eliminated, indicating excellent demulsification capability of **MS-4**.

4. Conclusion

In conclusion, a superhydrophobic melamine sponge **MS-4** was prepared *via* a one-pot dip coating method by reacting secondary amines in the sponge skeleton with stearic anhydride to form a hydrophobic layer on the sponge surface. **MS-4** exhibited excellent sorption capacities (up to 160 times its own mass), good recyclability (retention of over 93% after 50 sorption/squeezing cycles), exceptional stability under harsh conditions, superb selectivity for continuous oil/water separation using a vacuum pump-assisted device and outstanding demulsification ability. The facile and easily scalable fabrication of **MS-4** with cost-effective raw materials holds great promise of industrialization. It facilitates remediation of oil spills at a cost of ~ $1.0 per liter, which is considerably lower than the average clean-up cost of approximately $80 per liter [70]. Therefore, we believe the distinctive merits of this novel superhydrophobic sorption material would offer an efficient and economically viable solution for addressing large-scale oil spills.

CRediT authorship contribution statement

Zhihao Dong: Methodology, Investigation, Formal analysis, Writing – original draft, Visualization. **Wenzheng Feng:** Methodology, Investigation, Formal analysis. **Chi Huang:** Methodology, Investigation,

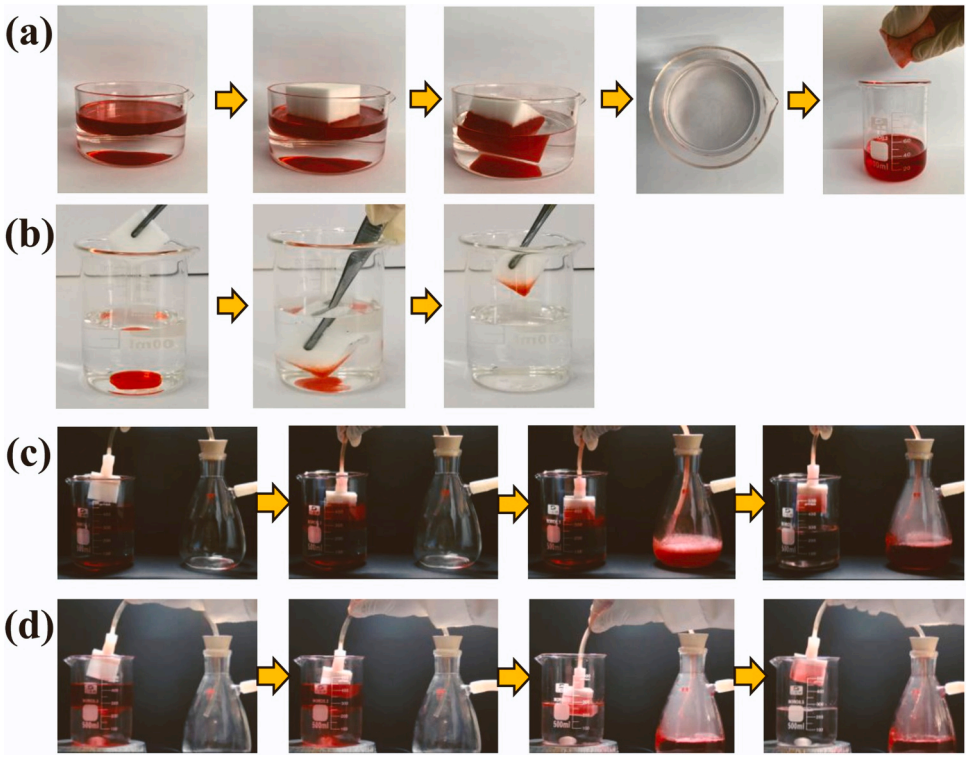

Fig. 8. Photographs of (a) the selective sorption and recovery of diesel (dyed with Sudan III) by **MS-4**; (b) the selective sorption of chloroform (dyed with Sudan III) by **MS-4**; (c) the continuous separation of still diesel/water mixture by **MS-4**; (d) the continuous separation of diesel/water mixture by **MS-4** under vigorous stirring.

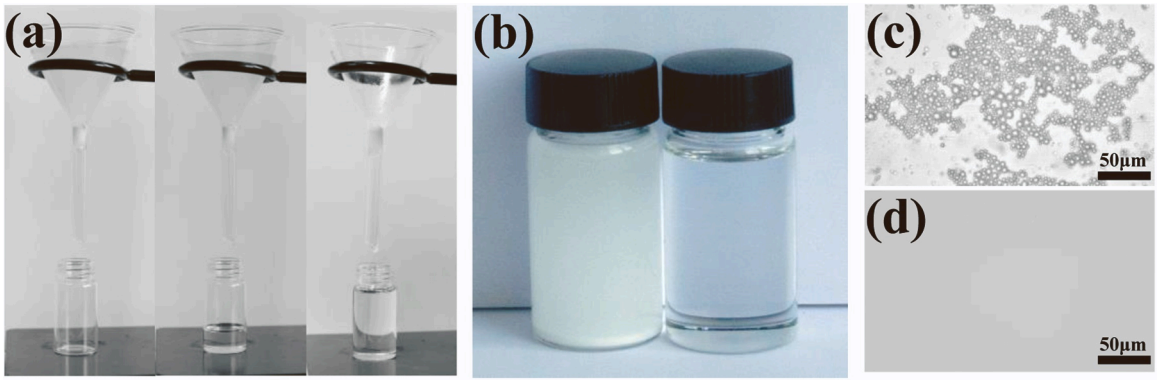

Fig. 9. Photographs of (a) the water-in-toluene emulsion separation process and (b) the emulsion before and after filtration; optical microscopy images of emulsion (c) and filtrate (d).

Formal analysis. **Hongpeng Lin:** Investigation. **Chunyan Jia:** Investigation. **Changliang Ren:** Conceptualization, Methodology, Validation, Formal analysis, Writing – review & editing, Supervision, Project administration, Funding acquisition.

Declaration of Competing Interest

The authors declare that they have no known competing financial interests or personal relationships that could have appeared to influence the work reported in this paper.

Data Availability

Data will be made available on request.

Acknowledgements

This work was supported by the National Natural Science Foundation of China (22001221), Shenzhen Science and Innovation Committee (JCYJ20210324123411030 and 2021Szvup067) and the Fundamental Research Funds for the Central Universities (20720210101).

Appendix A. Supporting information

Supplementary data associated with this article can be found in the online version at doi:10.1016/j.jece.2023.110614.

References

[1] S. Azizian, M. Khosravi, Advanced oil spill decontamination techniques, in: Interface Science and Technology, 30, Elsevier, 2019, pp. 283–332.
[2] Y. Yan, M. He, P. Zhou, X. Zeng, X. Huang, P. Pi, S. Xu, L. Wang, X. Wen, Sep. Purif. Technol. 304 (2023), 122374.

[3] Y. Yan, P. Zhou, S. Zhang, X. Yin, X. Zeng, P. Pi, Y. Nong, X. Wen, J. Water, Process. Eng. 49 (2022), 102942.
[4] V. Broje, A.A. Keller, J. Hazard. Mater. 148 (2007) 136–143.
[5] J. Aurell, B.K. Gullett, Environ. Sci. Technol. 44 (2010) 9431–9437.
[6] R. Pagnucco, M.L. Phillips, J. Environ. Manag. 225 (2018) 10–16.
[7] R.C. Prince, Environ. Sci. Technol. 49 (2015) 6376–6384.
[8] Q. Luo, D.Y. Hou, D.W. Jiang, W. Chen, Int. Biodeterior. Biodegrad. 32 (2021) 165–177.
[9] F.L. Motta, S.R. Stoyanov, J.B. Soares, Chemosphere 194 (2018) 837–846.
[10] C. Ren, J. Shen, F. Chen, H. Zeng, Angew. Chem. Int. Ed. 129 (2017) 3905–3909.
[11] J. Chang, Y. Shi, M. Wu, R. Li, L. Shi, Y. Jin, W. Qing, C. Tang, P. Wang, J. Mater. Chem. A 6 (2018) 9192–9199.
[12] W. Lei, D. Portehault, D. Liu, S. Qin, Y. Chen, Nat. Commun. 4 (2013) 1–7.
[13] L. He, W. Lei, D. Liu, Sep. Purif. Technol. 264 (2021), 118446.
[14] A. Jamsaz, E.K. Goharshadi, J. Mol. Liq. 307 (2020), 112979.
[15] A. Jamsaz, E.K. Goharshadi, Process Saf. Environ. Prot. 139 (2020) 297–304.
[16] H. Sun, Z. Xu, C. Gao, Adv. Mater. 25 (2013) 2554–2560.
[17] L. Sun, Z. Jiang, B. Yuan, S. Zhi, Y. Zhang, J. Li, A. Wu, Chem. Eng. Res. Des. 174 (2021) 71–78.
[18] J. Zhang, Q. Xue, X. Pan, Y. Jin, W. Lu, D. Ding, Q. Guo, Chem. Eng. J. 307 (2017) 643–649.
[19] H. Li, J. Zhang, L. Zhu, H. Liu, S. Yu, J. Xue, X. Zhu, Q. Xue, J. Hazard. Mater. 415 (2021), 125677.
[20] H. Li, J. Zhang, S. Gan, X. Liu, L. Zhu, F. Xia, X. Luo, Q. Xue, Adv. Funct. Mater., (2023).
[21] N.Y. Abu-Thabit, O.J. Uwaezuoke, M.H.A. Elella, Chemosphere 294 (2022), 133644.
[22] Q. Chen, L. Zhang, Y. Shan, Y. Liu, D. Zhao, Nanomater 12 (2022) 3527.
[23] R. Panickar, C.B. Sobhan, S. Chakravorti, Langmuir 37 (2021) 12501–12511.
[24] X. Qi, Z. Gao, C. Li, S. Wang, X. Zou, L. He, H. Cui, Z. Liu, J. Clean. Prod. 404 (2023), 136963.
[25] R. Wang, X. Zhu, L. Zhu, H. Li, J. Xue, S. Yu, X. Liu, S. Gan, Q. Xue, Sep. Purif. Technol. 289 (2022).
[26] L. Li, R. Chen, F. Wen, Y. He, L. Cheng, J. Ma, J. Mu, J. Appl. Polym. Sci. 140 (2023), e53875.
[27] Y.A. Patil, V.R. Mehta, D.R. Boraste, G.S. Shankarling, J. Environ. Chem. Eng. 9 (2021), 106603.
[28] V. Arunagiri, A. Prasannan, J. Udomsin, J.-Y. Lai, C.-F. Wang, P.-D. Hong, H. C. Tsai, Sep. Purif. Technol. 259 (2021), 118081.
[29] J. Xue, L. Zhu, X. Zhu, H. Li, C. Ma, S. Yu, D. Sun, F. Xia, Q. Xue, Sep. Purif. Technol. 259 (2021), 118106.
[30] Y. Pan, S. Huang, F. Li, X. Zhao, W. Wang, J. Mater. Chem. A 6 (2018) 15057–15063.
[31] H. Huang, C. Zhao, J. Li, J. Cheng, D. Xiang, J. Wei, Y. Yang, Z. Li, Y. Li, M. Qin, Colloids Surf. A Physicochem. Eng. Asp. 658 (2023), 130710.
[32] W. Chen, V. Karde, T.N. Cheng, S.S. Ramli, J.Y. Heng, Front. Chem. Sci. Eng. 15 (2021) 90–98.
[33] A.B.D. Cassie, S. Baxter, Trans. Faraday Soc. 40 (1944) 546–551.
[34] S. Wang, K. Liu, X. Yao, L. Jiang, Chem. Rev. 115 (2015) 8230–8293.
[35] V.H. Pham, J.H. Dickerson, ACS Appl. Mater. Interfaces 6 (2014) 14181–14188.
[36] O. Duman, C.Ö. Diker, S. Tunç, J. Environ. Chem. Eng. 9 (2021), 105093.
[37] P. Larkin, Infrared and Raman Spectroscopy: Principles and Spectral Interpretation, Elsevier, 2017.
[38] M.M. Radetić, D.M. Jocić, P.M. Jovančić, Z.L. Petrović, H.F. Thomas, Environ. Sci. Technol. 37 (2003) 1008–1012.
[39] Y. Deng, C. Peng, M. Dai, D. Lin, I. Ali, S.S. Alhewairini, X. Zheng, G. Chen, J. Li, I. Naz, J. Clean. Prod. 266 (2020), 121624.
[40] D. Ceylan, S. Dogu, B. Karacik, S.D. Yakan, O.S. Okay, O. Okay, Environ. Sci. Technol. 43 (2009) 3846–3852.
[41] M. Li, C. Bian, G. Yang, X. Qiang, Chem. Eng. J. 368 (2019) 350–358.
[42] J. Ge, H.Y. Zhao, H.W. Zhu, J. Huang, L.A. Shi, S.H. Yu, Adv. Mater. 28 (2016) 10459–10490.
[43] X. Wu, Y. Lei, S. Li, J. Huang, L. Teng, Z. Chen, Y. Lai, J. Hazard. Mater. 403 (2021), 124090.
[44] Y. Shui, Y. Xian, L. Chen, M. Li, Y. Yao, Q. Zhang, J. Appl. Polym. Sci. 137 (2020) 49306.
[45] Y. Fang, L. Yan, H. Liu, ACS Appl. Polym. Mater. 2 (2020) 3781–3788.
[46] Z. Lei, Y. Deng, C. Wang, J. Mater. Chem. A 6 (2018) 3258–3263.
[47] Z.-R. Jiang, J. Ge, Y.-X. Zhou, Z.U. Wang, D. Chen, S.-H. Yu, H.-L. Jiang, N.P. G. Asia, Mater 8 (2016) e253-e253.
[48] J. Wang, H. Wang, G. Geng, Mar. Pollut. Bull. 127 (2018) 108–116.
[49] C. Ruan, K. Ai, X. Li, L. Lu, Angew. Chem. Int. Ed. 126 (2014) 5662–5666.
[50] T. Chen, S. Zhou, Z. Hu, X. Fu, Z. Liu, B. Su, H. Wan, X. Du, Z. Gao, Colloids Surf. A Physicochem. Eng. Asp. 626 (2021), 127041.
[51] Y. Yang, H. Yi, C. Wang, ACS Sustain. Chem. Eng. 3 (2015) 3012–3018.
[52] S. Qiu, B. Jiang, X. Zheng, J. Zheng, C. Zhu, M. Wu, Carbon 84 (2015) 551–559.
[53] Q. Yao, P. Zhao, R. Li, C. Li, Y. Luo, G. Zhou, M. Yang, J. Chem. Technol. Biotechnol. 92 (2017) 1415–1420.
[54] A. Stolz, S. Le Floch, L. Reinert, S.M. Ramos, J. Tuaillon-Combes, Y. Soneda, P. Chaudet, D. Baillis, N. Blanchard, L. Duclaux, Carbon 107 (2016) 198–208.
[55] X. Zhou, Z. Zhang, X. Xu, X. Men, X. Zhu, Ind. Eng. Chem. Res. 52 (2013) 9411–9416.
[56] J. Chen, H. You, L. Xu, T. Li, X. Jiang, C.M. Li, J. Colloid Interface Sci. 506 (2017) 659–668.
[57] J. Zhang, R. Chen, J. Liu, Q. Liu, J. Yu, H. Zhang, X. Jing, P. Liu, J. Wang, Chemosphere 239 (2020), 124793.
[58] J. Li, Y. Chen, J. Gao, Z. Zuo, Y. Li, H. Liu, Y. Li, ACS Appl. Mater. Interfaces 11 (2018) 2591–2598.
[59] P. Makoś-Chełstowska, E. Słupek, A. Małachowska, J. Hazard. Mater. 425 (2022), 127972.
[60] X. Chen, J.A. Weibel, S.V. Garimella, Ind. Eng. Chem. Res. 55 (2016) 3596–3602.
[61] Q. Ke, Y. Jin, P. Jiang, J. Yu, Langmuir 30 (2014) 13137–13142.
[62] Z. Wan, Y. Liu, S. Chen, K. Song, Y. Peng, N. Zhao, X. Ouyang, X. Wang, Colloids Surf. A Physicochem. Eng. Asp. 546 (2018) 237–243.
[63] E.-C. Cho, Y.-S. Hsiao, K.-C. Lee, J.-H. Huang, RSC Adv. 5 (2015) 53741–53748.
[64] X. Ye, Y. Cui, L. Ke, K. Gao, X. Huang, B. Shi, Colloids Surf. A Physicochem. Eng. Asp. 551 (2018) 9–16.
[65] Y. Feng, Y. Wang, Y. Wang, J. Yao, J. Mater. Chem. A 5 (2017) 21893–21897.
[66] K. Zheng, W. Li, S. Zhou, G. Huang, J. Hazard. Mater. 429 (2022), 128348.
[67] A. Jamsaz, E.K. Goharshadi, A. Barras, M. Ifires, S. Szunerits, R. Boukherroub, Sep. Purif. Technol. 274 (2021).
[68] G. Zhai, J. Wu, Z. Yuan, H. Li, D. Sun, Inorg. Chem. 62 (2023) 5447–5457.
[69] D.D. Ejeta, C.-F. Wang, S.-W. Kuo, J.-K. Chen, H.-C. Tsai, W.-S. Hung, C.-C. Hu, J.-Y. Lai, Chem. Eng. J. 402 (2020), 126289.
[70] R. Bousso, USA Today 16 (2018).